Neurovascular Coupling Analysis Based on Multivariate Variational Gaussian Process Convergent Cross-Mapping

Renfei Zhu, Qingshan She, Rihui Li, Tongcai Tan, and Yingchun Zhang, *Senior Member, IEEE*

Abstract—**Neurovascular coupling (NVC) provides important insights into the intricate activity of brain functioning and may aid in the early diagnosis of brain diseases. Emerging evidences have shown that NVC could be assessed by the coupling between electroencephalography (EEG) and functional near-infrared spectroscopy (fNIRS). However, this endeavor presents significant challenges due to the absence of standardized methodologies and reliable techniques for coupling analysis of these two modalities. In this study, we introduced a novel method, i.e., the collaborative multi-output variational Gaussian process convergent cross-mapping (CMVGP-CCM) approach to advance coupling analysis of EEG and fNIRS. To validate the robustness and reliability of the CMVGP-CCM method, we conducted extensive experiments using chaotic time series models with varying noise levels, sequence lengths, and causal driving strengths. In addition, we employed the CMVGP-CCM method to explore the NVC between EEG and fNIRS signals collected from 26 healthy participants using a working memory (WM) task. Results revealed a significant causal effect of EEG signals, particularly the delta, theta, and alpha frequency bands, on the fNIRS signals during WM. This influence was notably observed in the frontal lobe, and its strength exhibited a decline as cognitive demands increased. This study illuminates the complex connections between brain electrical activity and cerebral blood flow, offering new insights into the underlying NVC mechanisms of WM.**

Index Terms—**Neurovascular coupling (NVC), multi-output Gaussian process, convergent cross-mapping, electroencephalography (EEG), functional near-infrared spectroscopy (fNIRS), working memory.**

I. INTRODUCTION

THE human brain maintains its normal functioning by regulating vascular supply to meet the metabolic demands of neurons under different conditions [1]. Neurovascular coupling (NVC) is a major factor in ensuring proper blood supply to the brain, representing the tight connection between neural activity and cerebral blood flow [2]. In recent years, there has been considerable interest in understanding the NVC mechanisms in cognitive tasks [3], [4], [5], particularly in working memory (WM). WM, a cognitive ability to temporarily store and manipulate information, is one of the important cognitive processes in everyday human life. The coupling between neural activity and cerebral blood flow plays a crucial regulatory role in WM. The n-back task is one of the most common experimental paradigms in WM research. This task requires participants to respond when a stimulus appears that is the same as the one presented in the previous n-th trial, with n typically predetermined as 1, 2, or 3 [6]. The n-back task is thought to be used to boost the capacity of the brain's WM for a short time.

Electroencephalography (EEG) and functional near-infrared spectroscopy (fNIRS) are common neuroimaging techniques. EEG is widely used to monitor brain function by capturing neuronal electrical activity through electrodes placed over the scalp. EEG has high temporal resolution but limited spatial resolution [7], [8], [9], [10], as it cannot detect neural activity from deep cortical regions. fNIRS uses infrared light absorption and scattering to measure changes in the concentration of oxygenated hemoglobin (HbO) and deoxygenated hemoglobin (HbR) in brain tissue [11], [12]. It is non-invasive, portable, and has higher spatial resolution compared to EEG [13], [14]. The unique advantages of these two neuroimaging techniques,

Renfei Zhu and Qingshan She are with the School of Automation, Hangzhou Dianzi University, Hangzhou, Zhejiang 310018, China, and also with the International Joint Research Laboratory for Autonomous Robotic Systems, Hangzhou, Zhejiang 310018, China (e-mail: qsshe@hdu.edu.cn).

Rihui Li is with the Center for Cognitive and Brain Sciences and the Department of Electrical and Computer Engineering, University of Macau, Macau, SAR, China (e-mail: rihuili@um.edu.mo).

Tongcai Tan is with the Department of Rehabilitation, Medicine, Zhejiang Provincial People's Hospital, People's Hospital of Hangzhou Medical College, Hangzhou, Zhejiang 310014, China (e-mail: 29ttc@sina.com).

Yingchun Zhang is with the Department of Biomedical Engineering, Desai Sethi Urology Institute, Miami, FL 33136 USA, and also with Miami Project to Cure Paralysis, University of Miami, Coral Gables, FL 33146 USA (e-mail: y.zhang@miami.edu).

with their complementary temporal and spatial characteristics [14], [15], [16], [17], [18], make them valuable tools for studying the mechanisms of NVC [19].

In previous studies [20], [21], [22], [23], research based on simultaneous acquisition of EEG and fNIRS signals has mainly focused on correlation analysis. Several studies have used Pearson correlation method to explore the association between neural activity and hemodynamics under WM [20], [21]. Dashtestani et al. [22] applied canonical correlation analysis (CCA) to investigate the coupling between EEG and fNIRS signals at the spatiotemporal level. Chiarelli et al. [23] combined EEG signals with the generalized linear model (GLM) and utilized EEG signals characteristics to model fNIRS signals. However, traditional coupling analysis methods, such as Pearson correlation coefficients or mutual information (MI) measures [24], [25], typically analyze samples based on mathematical definitions, disregarding the dynamic structure of time series and directional coupling. Borgheai et al. [26] also emphasized the importance of analyzing not only the correlation but also the causality between EEG signals and fNIRS signals. Sugihara et al. [27] proposed the theory of convergent cross-mapping (CCM), which has advantages in addressing causal relationship problems between nonlinear systems. The CCM method was first applied in the brain's functional connectivity analysis in the field of neural signal analysis [28], [29], [30], [31]. In recent research, Ghouse et al. [32] introduced the CCM method into the study of EEG-fNIRS coupling analysis, providing a new direction for causal analysis of NVC.

Although CCM has been successfully applied in previous research, its sensitivity to noise hinders its general applicability in the analysis of general coupling systems [33]. To mitigate the influence of process noise, some studies improved the CCM method. The frequency-domain CCM method [31] has been proposed for analyzing functional connectivity in the brain, which estimates causal driving effects by mapping the power spectra between two time series. Stavroglou et al. [34] introduced an analysis method based on symbolic dynamics to validate the CCM through a priori defined causal interaction models. In recent years, concepts such as MI, entropy, and Gaussian processes have also been introduced to extend CCM. For instance, permutation pattern-based MI estimation was employed to achieve cross-mapping capability [35]. One study [36] combined the concept of Gaussian processes with the CCM method, transforming causal inference into a conditional probability problem. Despite the emerging effort taken to improve the robustness of CCM, significant research gaps remain in terms of the reliability of causal direction determination and reducing information loss.

To address the limitations of the CCM method, this study proposed a novel method, the collaborative multi-output variational Gaussian process convergent cross-mapping (CMVGP-CCM), to construct a convergent cross-mapping function that effectively compensated for the information loss in the single-output Gaussian processes. Building upon this, a coupling analysis framework based on CMVGP-CCM was introduced for causal analysis of EEG-fNIRS signals. This framework was applied to investigate the NVC mechanism

in the n-back paradigm, so as to target and quantitatively understand the information transmission between EEG and fNIRS, and contributing to the understanding of neural mechanism in WM.

The specific contributions of this article are summarized as follows:

1) We proposed the CMVGP-CCM method. Unlike existing causal relationship measurement methods, CMVGP-CCM was able to capture the potential correlations among multiple input signals (i.e., EEG and fNIRS), thereby reducing information loss.

2) The algorithm of the proposed method was thoroughly described and validated on simulated datasets. Simulation results demonstrated how the quality of causal inference is affected by coupling strength, data length, and noise, thus proving the robustness and effectiveness of the CMVGP-CCM method.

3) We applied the CMVGP-CCM method to the causal analysis of EEG-fNIRS signals during the n-back paradigm, demonstrating differences in NVC under varying cognitive difficulties.

The structure of this paper is as follows. Section II introduced the experimental data and methods used in this paper. Section III presented the results of the proposed method in simulation experiments and the analysis of NVC. In Section IV, the experimental results were discussed. Section V provided the conclusions.

II. Experimental Materials and Methods

A. EEG-fNIRS Dataset and Paradigm

A publicly available dataset [37] consisting of EEG-fNIRS data collected during WM tasks was used analysis in this study. The dataset comprised 26 healthy right-handed participants, including 9 males and 17 females, with an average age of 26.1 ± 3.5 years. Each participant performed nine series of n-back tasks, with each set including a 2-second instruction for the task type (0-, 2-, or 3-back), a 40-second task period, and a 20-second rest period. Fig. 1a illustrates the workflow of a single series.

The fNIRS data were collected using NIRScout at a sampling frequency of 10.4 Hz. A total of 16 sources and 16 detectors were placed, resulting in 36 fNIRS channels (see Fig. 1b) according to the international 10-5 system. All channels had a source-detector distance of 30 mm.

The EEG data was sampled at a rate of 1000 Hz and collected using the multichannel BrainAmp EEG amplifier. 30 active electrodes (refer to Fig. 1b) were placed on an elastic fabric cap according to the international 10-5 system, with TP9 as the reference electrode and TP10 grounded.

B. Data Preprocessing

In this study, a total of 30 EEG channels and 36 fNIRS channels were simultaneously collected from the entire brain. Based on previous research [37], brain regions related to WM: prefrontal, left-right motor and parietal regions were taken into account. Considering the spatial distribution of
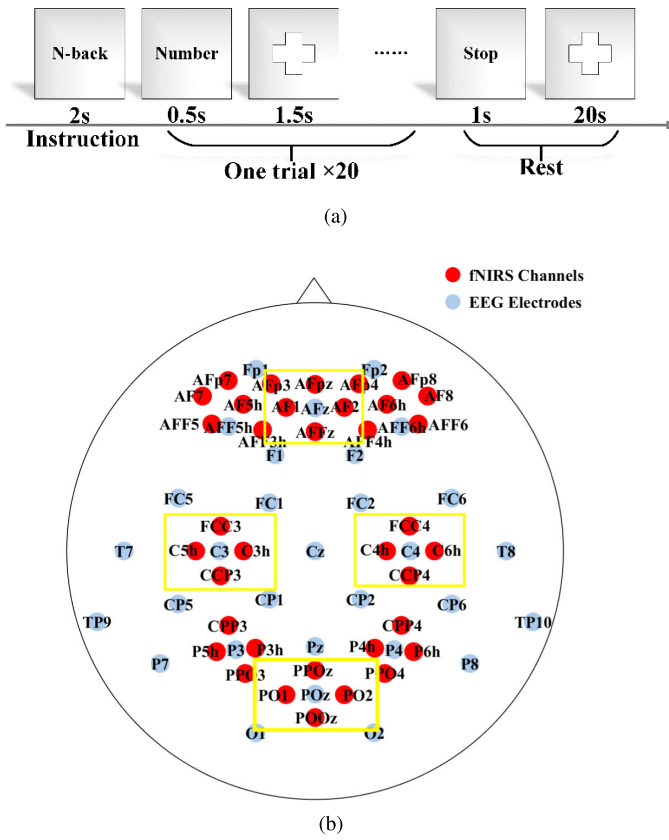
(a)

(b)

Fig. 1. (a) The experimental procedure of the *n*-back paradigm. (b) Electrodes placement: EEG electrodes (blue) and fNIRS channels (red). The channels in the yellow box were selected.

channels [32], [38], representative EEG channels (AFz, C3, C4, POz) were selected in the middle prefrontal, motor and parietal regions in subsequent processing, as well as four fNIRS channels adjacent to each selected EEG channel (refer to Fig. 1b) to ensure spatial consistency and capture nerve and vascular activities more comprehensively. All EEG and fNIRS data preprocessing was done through the EEGLAB toolbox and custom MATLAB scripts [39], [40].

The raw fNIRS data was downsampled to 10 Hz, converted to optical density, and finally converted to HbR and HbO using the modified Beer-Lambert law (MBLL). High-frequency noise and physiological noise were removed through low-pass filtering using a 6th-order zero-phase Butterworth filter with a cut-off frequency of 0.2 Hz. To further obtain clean data, variational mode decomposition (VMD) was used to remove motion artifacts [41]. The filtered data was segmented into time series ranging from −5s to 60s and baseline correction. For each brain area, the average of the four fNIRS channels was taken.

The raw EEG data was downsampled to 200 Hz, bandpass filtered with a passband of 1-45 Hz, and notch filtered at 50 Hz to remove power line noise. The EEG signals were then re-referenced using an average reference. To mitigate artifacts, independent component analysis (ICA) was used to remove interference sources. The filtered data was segmented into time series ranging from −5 s to 60 s. In order to further remove noises and obtain cleaner frequency band signals, the EEG

signals were decomposed into classical EEG frequency bands (delta: 1-4 Hz, theta: 4-8 Hz, alpha: 8-13 Hz, beta: 13-30 Hz, gamma: 30-45 Hz) using VMD. Finally, a short-time Fourier transform (STFT) was conducted with a window length of 8 s and a step size of 0.02 s to obtain the time course of EEG signal sampled at 10 Hz, corresponding to the frequency of the fNIRS time series.

C. The Proposed Method

1) Convergent Cross-Mapping Theory: CCM is mainly applicable to the analysis of weak coupling relationships in nonlinear dynamic systems. The basic principle of cross mapping is to reconstruct the system state space from two time series variables through time delay embedding, and to quantify the corresponding relationship between them using nearest neighbor prediction [42]. The aforementioned fundamental principle is the foundation of CCM and its improved methods.

CCM can identify both unidirectional causal relationships and bidirectional causal relationships when variables are mutually coupled. Additionally, CCM addresses the cases involving systems with interdependencies that are not covered by granger causality (GC).

2) CMVGP-CCM Method: The Gaussian process framework allows placing probability density functions at each point in the reconstructed state space, thus transforming cross-mapping into likelihood posterior probability distribution. The variational Gaussian process convergent cross-mapping (VGP-CCM) method [36] introduced the Gaussian process and variational Bayesian optimization, which had good robustness and the ability to suppress false positives (i.e., significance judgment of causal direction). However, this approach is not suitable for multitasking scenarios. When the amount of data is small, the advantages of the algorithm cannot be fully reflected. To address these limitations, we proposed the CMVGP-CCM method. The proposed CMVGP-CCM method assumes the existence of latent relationships among multiple time series and complements the single-output Gaussian process with latent correlated variables and specific variables of multiple time series. This enables capturing correlations between multiple sets of time series simultaneously, reducing information loss by discovering latent correlations among inputs, and exhibiting good robustness to noise.

Based on the characteristics of multidimensional Gaussian processes, there is a parallel relationship between the calculation of multiple groups of variables. The following will be introduced from the perspective of individual dimensions.

The following are the step-by-step instructions to calculate causal strength:

Step 1: Reconstruction of the state space $\varphi(X)$ and $\varphi(Y)$.

In particular, the selection methods of the important parameters of state-space reconstruction include:

a. Time delay tau: Calculates the autocorrelation function of the input signal. When the autocorrelation function reaches the set threshold (default is 0.5) at a certain lag value τ, the lag value τ is selected as the time delay parameter.

b. Embedding dimension E: According to the false nearest neighbors (FNN) criterion, two points adjacent in a

low-dimensional embedding space may be relatively far apart in a higher-dimensional space. By increasing the embedding dimension, the proportion of false nearest neighbors is calculated, and when it is less than the tolerance (default is 0.01), the optimal embedding dimension is determined.

The observed EEG time series X has x_i sampling points. Based on a m_x-dimensional delay coordinate embedding, the i-th state $\varphi(X)_i$ of X as follow:

$$\varphi(X)_i = \{x_i, x_{i+\tau}, \ldots, x_{i+(m_x-1)\tau}\}, i \in 1, 2, \ldots, N. \quad (1)$$

where τ represents the time delay, m_x is the number of embedding dimensions, and N represents the number of observed states. The reconstructed state space is obtained as $R^{N \times m}$. The above steps apply similarly to the fNIRS signal Y.

Step 2: Performing maximum likelihood estimation for time series to find the optimal kernel function.

In the function space, the state space $\varphi(X)$ of the EEG signal and the state space $\varphi(Y)$ of the fNIRS signal are considered realizations of random Gaussian processes. A square exponential covariance function [43] with deterministic autocorrelation and hyperparameters $\theta_x^{ard} = \{A, l_1, l_2, \ldots, l_{m_x}\}$ is chosen as the prior kernel function.

We then construct the $N \times N$ kernel matrix by pairing all possible observed states:

$$K_x = \{\beta_o K[\varphi(X)_i, \varphi(X)_j + \beta_L K[\varphi(U)_i, \varphi(U)_j]] + \beta_S K[\varphi(S)_i, \varphi(S)_j]\}. \quad (2)$$

$$K_{xy} = \{K[\varphi(X)_i, \varphi(Y)_j]\}. \quad (3)$$

$$K_{yx} = K_{xy}^T, i, j = 1, 2, \ldots, N. \quad (4)$$

Similarly, the state space of $\varphi(Y)$ can be used to construct the kernel matrix K_y. The definitions of U and S are shown in **Fig. 2**. U is extracted from the time series $\varphi(X_t)_i$, $t = 1, 2, \ldots, T$ of T EEG inputs by performing principal component analysis (PCA), and S is obtained by the difference with the multidimensional input and U. Both parts are reconstructed by the correlation matrix with the inputs. To simplify the equation, the subscripts for U and S variables are not explicitly shown in Eq. (2). K_x and K_y are referred to as the autocovariance matrices, while K_{xy} and K_{yx} are referred to as the cross-covariance matrices.

Set σ_x as the prior knowledge of noise, the multivariate Gaussian distribution can be constructed based on Eqs. (3) and (4) as follows:

$$P\left[\varphi(X), \varphi(Y); \theta_x^{ard}, \sigma_x, j\right] = N\left([0, 0], \begin{bmatrix} K_x + \sigma_x I & K_{xy} \\ K_{yx} & K_y \end{bmatrix}\right). \quad (5)$$

All hyperparameters mentioned in Step 2 are optimized through Bayesian optimization.

Step 3: Obtain the posterior probability distributions of the EEG time series X and fNIRS time series Y. Let θ_x be a set of kernel parameters, and $\hat{X}$ and $\hat{Y}$ be the zero distributions for non-coupled processes. To eliminate the dependence of conditional samples on X, uses $M(\theta_x)$ based on mean-field
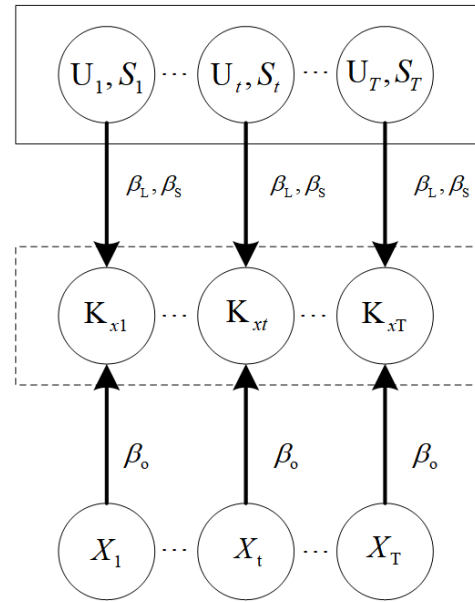

Fig. 2. The graphical model of the collaborative multi-output Gaussian process kernel matrix constructed. In this model, X_t represents the t-th time series, U_t and S_t represent potentially relevant and specific components extracted from multiple time series sets, respectively, and β_L, β_S and β_o are the corresponding weight values. K_{xt} is the resulting autovariance matrix.

approximation $P(\theta_x \mid X)$ to obtain the following posterior distribution:

$$\hat{\kappa} \approx \frac{\int P(\hat{Y} \mid \theta_x) M(\theta_x) d\theta_x}{\int P(\hat{X} \mid \theta_y) M(\theta_y) d\theta_y}. \quad (6)$$

Step 4: For the causal strength $\hat{\kappa}$ obtained from the posterior probability, the most likely causal direction can be determined using the Bayesian model comparison test. The obtained statistical measure K is constrained to the open interval $(-1, 1)$ using hyperbolic tangent. K is used as an indicator to measure causal relationships. When $K > 0$, there is stronger evidence that the causal direction is EEG→fNIRS, when $K < 0$, the causal direction is fNIRS→EEG. Otherwise, there is no causal relationship between EEG and fNIRS.

Step 5: Verifying the reliability of the results through the null distribution.

To determine if the probability of the causal statistic in the null distribution is less than p, the Kolmogorov-Smirnov test is performed on the samples in $K(X, Y)$. p is usually set to 0.05.

D. Simulation Experiments

The effectiveness and reliability of the proposed method were verified by the simulation model from three aspects: determination of causal direction ((**Simulation 1**)), robustness to noise ((**Simulation 2**)) and data length ((**Simulation 3**)).

1) Lorenz-Rossler Systems: To validate the efficacy of the proposed method in determining the causal driving direction, Lorenz X and Rossler Y chaotic systems with nonlinear unidirectional coupling driven by Wiener process were simulated.
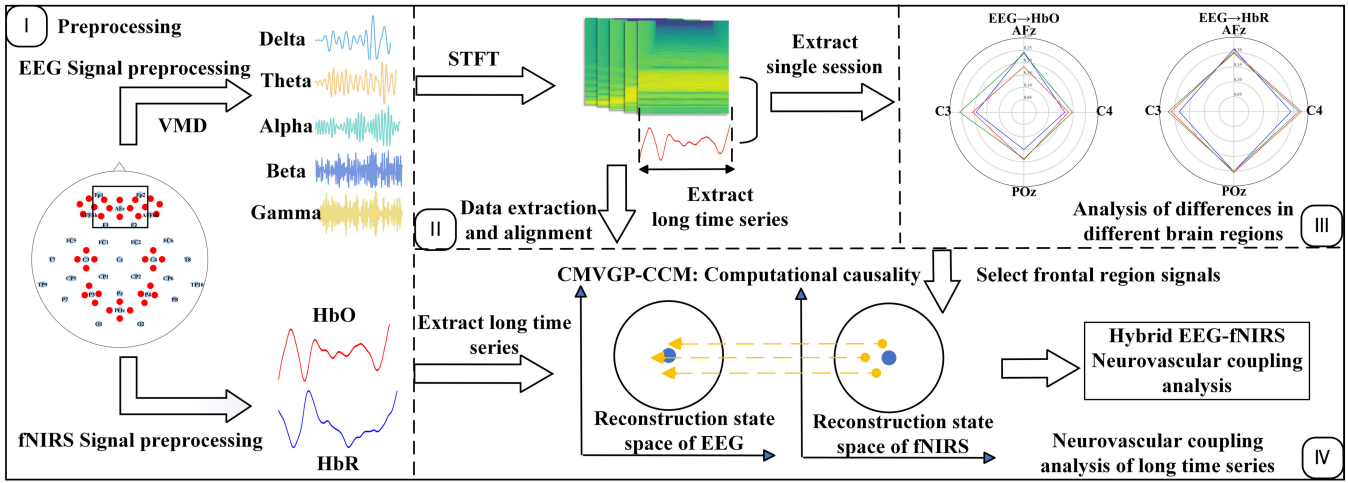
Fig. 3. The NVC analysis framework based on CMVGP-CCM. The framework consists of four parts: I. Data preprocessing. II. Data extraction and data length alignment. III. The causal analysis of EEG-fNIRS based on different brain regions. IV. The NVC analysis of long time series. Part IV shows the cross-mapping illustration when EEG has a causal effect on fNIRS.

TABLE I
PARAMETERS USED TO INDUCE DETERMINISTIC CHAOS IN LORENZ-ROSSLER SYSTEMS

	Parameter	Value
Lorenz	σ	10
	ρ	28
	β	2.67
	σ_L	10^{-6}
Rossler	ω	0.985
	a	0.15
	b	0.2
	c	10
	σ_R	0.005
Wiener process	dW	$N(0,1)$
	dt	0.001

The unidirectional coupling system is represented as follows:

$$\begin{cases} dX_0 = (\sigma(X_1 - X_0) + \varepsilon_y X_0(Y_0 - 1)dt)dt + \sigma_L(t)dW_{X_0}. \\ dX_1 = (X_0(\rho - X_2) - X_1)dt + \sigma_L(t)dW_{X_1}. \\ dX_2 = (X_0 X_1 - \beta X_2)dt + \sigma_L(t)dW_{X_2}. \\ dY_0 = (-\omega Y_1 - Y_2 + \varepsilon_x Y_0(X_0 - 1))dt + \sigma_R(t)dW_{Y_0}. \\ dY_1 = (\omega Y_0 + aY_1)dt + \sigma_R(t)dW_{Y_1}. \\ dY_2 = (b + Y_2(Y_1 - c))dt + \sigma_R(t)dW_{Y_2}. \end{cases}$$
(7)

where $\{\varepsilon_x, \varepsilon_y\}$ determines the coupling relationship between the Lorenz and Rossler systems. The parameters for Lorenz and Rossler systems are shown in **Table 1**.

To investigate the impact of coupling strength on the directionality of causal inference (**Simulation 1**) and ensure reliable results, we selected multiple sets of different $\{\varepsilon_x, \varepsilon_y\}$. For each set of parameters, 30 implementations of the dynamic system were generated and 9 comparisons ($X_i \rightarrow Y_j, i, j = 1, 2, 3$) were performed for the six variables of the two systems, resulting in a total of 270 outcomes.

2) Logistic Map Processes: As a nonlinear dynamical model system, the logistic map exhibits both regular periodic behavior and deterministic chaos, making it an ideal model for testing the performance of CCM and its improved methods [44].

Gaussian white noise based on a normal distribution and external driving signals were introduced into the general logistic map model to simulate the coupling relationship between physiological signals. The constructed time series variables x and y are as follows:

$$x_{t+1} = x_t[r_x(1 - x_t) - \beta_{xy} y_t] + \varepsilon_{x,t}.$$
(8)

$$y_{t+1} = y_t[r_y(1 - y_t) - \beta_{yx} x_t] + \varepsilon_{y,t}.$$
(9)

where ε is a random variable sampled from a normal distribution $N(0, \sigma^2)$, representing disturbances from the environment.

We set $r_x = 3.8$ and $r_y = 3.5$. For simplicity, only the unidirectional coupling from x to y was considered (i.e., $\beta_{xy} = 0$ and $\beta_{yx} = 0.1$). The reliability of the proposed method was verified by setting different σ (**Simulation 2**) and data length (**Simulation 3**) variables.

E. Analysis of EEG-fNIRS Neurovascular Coupling in Working Memory

In order to conduct NVC analysis and investigate the causal relationship between EEG-fNIRS synchronous acquisition signals, we proposed the NVC analysis framework based on CMVGP-CCM (refer to **Fig. 3**).

After preprocessing, we extracted the group-averaged time series data of the selected EEG and fNIRS channels from 25 participants (participant 4 excluded due to data quality issues) at different cognitive difficulties. The effects of different cognitive loads on different brain regions on the causal relationship between EEG and fNIRS signals were studied using group average data. We then performed long-term NVC analysis of prefrontal regions strongly associated with WM. To ensure the reliability of the results while reducing the computational memory usage of CMVGP-CCM, the time series of the first five sessions for each cognitive task were

TABLE II
STATISTICAL ANALYSIS FOR CAUSAL DRIVING DIRECTION
(LORENZ → ROSSLER EQUATIONS $L \to R$, ROSSLER →
LORENZ EQUATIONS $R \to L$) INFERENCE

	VGP-CCM		CMVGP-CCM	
Chaotic System	$L \to R$	$R \to L$	$L \to R$	$R \to L$
$\varepsilon = (0.00, 0.00)$	0	9	0	9
$\varepsilon = (0.00, 0.133)$	0	1	0	**27**
$\varepsilon = (0.00, 0.20)$	0	21	0	**59**
$\varepsilon = (0.00, 0.266)$	0	74	0	**100**
$\varepsilon = (0.00, 0.40)$	0	131	0	**183**
$\varepsilon = (0.00, 0.50)$	0	158	0	**164**
$\varepsilon = (2.00, 0.00)$	166	0	**214**	0
$\varepsilon = (4.00, 0.00)$	178	0	**207**	0

$\{0, \varepsilon_y\}$ sets the causal direction $R \to L$, $\{\varepsilon_x, 0\}$ is $L \to R$.

Fig. 4. The change of causal statistic K of CMVGP-CCM method under different coupling strength. The results from X_3 to Y_1, Y_2, and Y_3 as examples.

selected for analysis (3250 sampling points). Based on the CMVGP-CCM method, the causal delay effect and causal intensity of EEG-fNIRS in different frequency bands and different n-back tasks were analyzed.

F. Statistical Analysis

Statistical analysis was used to analyze the results of simulation experiments and real EEG-fNIRS data. The significance p-values of all causal strength statistics were obtained from the null hypothesis test based on the random rearrangement method. All statistical analyses of EEG-fNIRS were performed by SPSS software. One-way analysis of variance (ANOVA) was used to determine whether the increase of cognitive load had significant effects on neurovascular coupling in different brain regions and different frequency bands. In long time-series experiments, non-parametric methods were employed for statistical analysis of the results. The Kruskal-Wallis non-parametric test was used to describe the significance of the results, and Bonferroni correction was used to make multiple comparison corrections to ensure result reliability.

III. RESULTS

A. Simulation Results

We verified the reliability and robustness of CMVGP-CCM through **Simulation 1**, **Simulation 2**, and **Simulation 3**, and compared them with the CCM and VGP-CCM methods. To unify the evaluation criteria, the causal estimation of CCM and VGP-CCM methods was also constrained to statistical measures within the range of $(-1, 1)$ using hyperbolic tangent. Significant p-values were obtained through null hypothesis testing. The results are as follows:

Simulation 1 investigated the specificity of CMVGP-CCM in inferring causal directions by adjusting the coupling parameter and compares the results with the VGP-CCM method. The p values were represented using the null distribution. **Table II** reports the number of causal inference outcomes with p<0.05 in the 270 groups. The experimental results demonstrated that as the coupling parameters increased, the CMVGP-CCM method was easier to obtain significant results, and performed better under low coupling conditions. Moreover, both the VGP-CCM and CMVGP-CCM methods
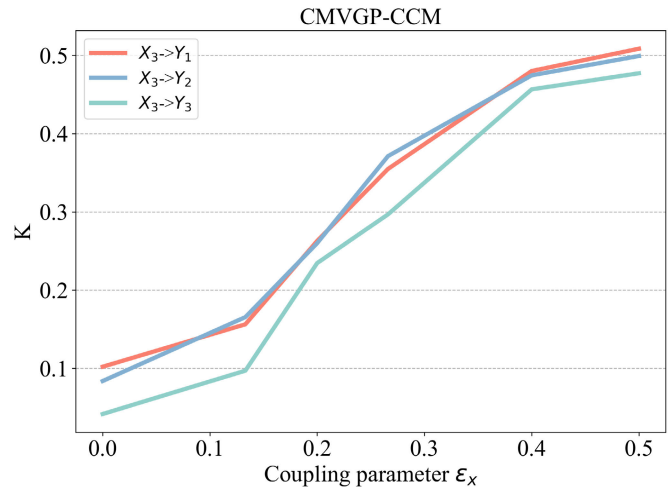
made fewer erroneous directional statements. CMVGP-CCM reported a specificity of 100% in the case of Rossler driving Lorenz, while VGP-CCM showed a specificity of 99.74%. Both CMVGP-CCM and VGP-CCM exhibited a specificity of 100% in the case of Lorenz driving Rossler. For the rejection of the hypothesis of either direction, CMVGP-CCM achieved a specificity of 99.06%, while VGP-CCM yielded a specificity of 98.64%. **Fig. 4** shows that the causal strength reported by CMVGP-CCM increases with the value of the coupling parameter. The proposed method can effectively identify the causal drivers between Lorenz-Rossler systems.

Almost all physiological data contains some level of noise. In **Simulation 2**, as the σ value increased, more noise was introduced, and metrics of the three methods showed a decreasing trend. In **Fig. 5a**, the CMVGP-CCM method has the smallest downward trend and good robustness, and the measured value of the CMVGP-CCM method is significantly higher than that of the CCM method (p<0.001).

In **Simulation 3**, the focus was on data length. **Fig. 5b** compares the convergence ability of the three methods in terms of data length. The causal strength of the CMVGP-CCM method converged when the data length was 850, while the other two methods converged at longer data lengths. **Simulation 3** further proved that CMVGP-CCM had a higher measurement value than the CCM method. In the case of extremely short time series, none of the three methods could provide reliable evidence of causal direction, which might have been due to the large uncertainty in the state space reconstruction at that time. The convergence of CMVGP-CCM was more robust than that of VGP-CCM. Compared with the CCM method, the CMVGP-CCM method produced lower coupling strength estimation under short time series conditions.

B. Neurovascular Coupling Analysis Results

Coupling analysis of EEG-fNIRS data includes two parts: brain region differences in short-time series, frequency band differences in long-time series. The results of these analyses are presented below.
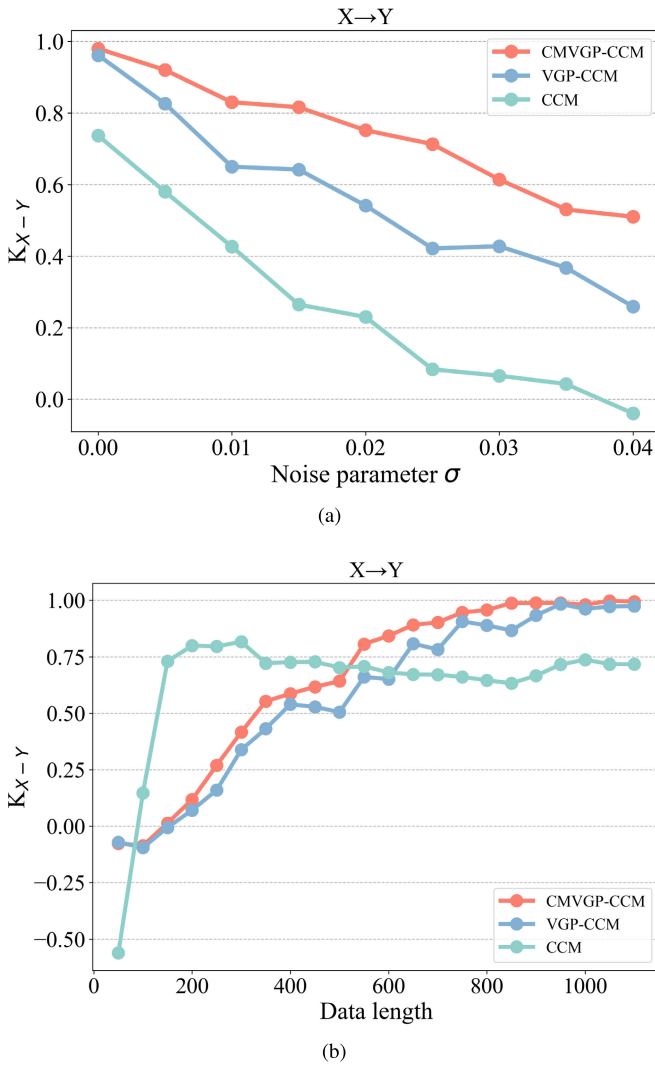
Fig. 5. The change of causal statistic K of CMVGP-CCM, VGP-CCM and CCM methods under different parameters. (a) Noise intensity variation. (b) Data length variation.
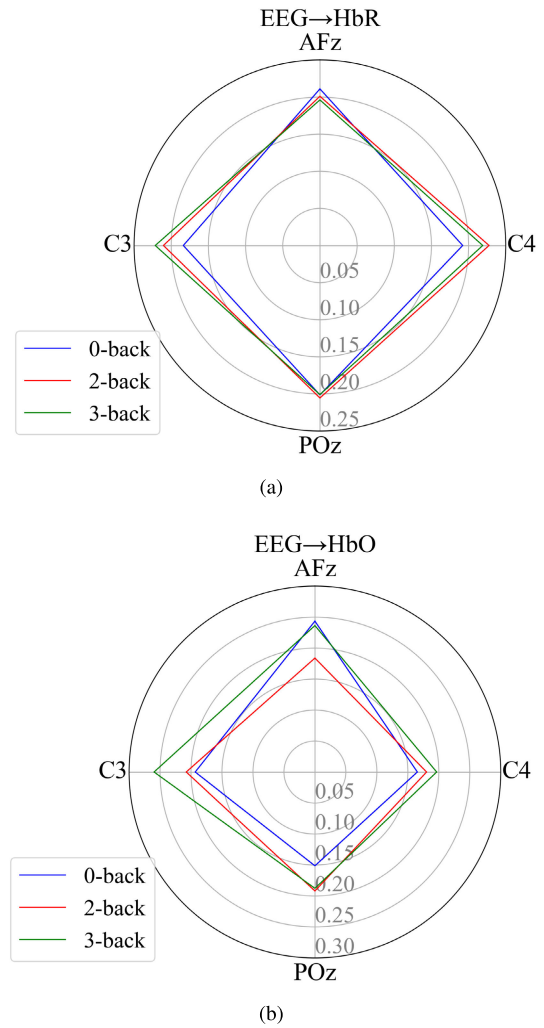

Fig. 6. The Causal driving strengths between EEG and fNIRS signals under different cognitive loads in different brain regions. (a) From EEG to HbR. (b) From EEG to HbO. EEG channels are used to refer to different brain regions, such as AFz for the prefrontal region.

It should be noted that the CMVGP-CCM was computed for the causal driving direction from EEG to fNIRS since hemodynamic response was internally driven by the neuronal activity. A value greater than 0 indicated a casual direction from EEG to fNIRS, otherwise it was from fNIRS to EEG. In the subsequent description, the causal driving effect of EEG signals on fNIRS signals is defined as $NVC_{EEG \rightarrow fNIRS}$.

Fig. 6 illustrates the causal strength differences between EEG and fNIRS signals under different cognitive tasks and brain regions. $NVC_{EEG \rightarrow HbR}$ of the middle prefrontal region (AFz-AFpz, AF1, AF2, AFFz) decreased with the increase of cognitive load, and $NVC_{EEG \rightarrow HbO}$ decreased first and then increased. With the increase of cognitive load, $NVC_{EEG \rightarrow HbR}$ and $NVC_{EEG \rightarrow HbO}$ increased in the left motor area (C3-FCC3, CCP3, C5h, C3h), and first increased and then decreased in the parietal area (POz-PPOz, POOz, PO1, PO2). Right motor area (C4-FCC4, CCP4, C4h, C6h) $NVC_{EEG \rightarrow HbO}$ increased with the increase of cognitive load, and $NVC_{EEG \rightarrow HbR}$ increased first and then decreased. The left and right motor brain regions showed lateralization. $NVC_{EEG \rightarrow fNIRS}$ of different brain regions in different

frequency bands and the results of one-way ANOVA are shown in Table III. Cognitive load had a significant effect on $NVC_{EEG \rightarrow HbR}$ in the middle prefrontal theta and alpha bands and $NVC_{EEG \rightarrow HbO}$ in all bands. $NVC_{EEG \rightarrow HbO}$ in all frequency bands decreased first and then increased, while $NVC_{EEG \rightarrow HbR}$ in theta and alpha bands decreased with increasing cognitive load. For the left motor region, cognitive load had a significant effect on $NVC_{EEG \rightarrow HbR}$ in the beta band and $NVC_{EEG \rightarrow HbO}$ in the gamma band. The two trends are opposite. For the right motor region, cognitive load had a significant effect on $NVC_{EEG \rightarrow HbO}$ in four frequency bands except delta. $NVC_{EEG \rightarrow HbO}$ in theta and alpha bands increased with the increase of cognitive load, while $NVC_{EEG \rightarrow HbO}$ in beta and gamma bands decreased and then increased. The effects of cognitive load on delta, theta and alpha bands of parietal lobe were significant. $NVC_{EEG \rightarrow HbR}$ in theta and alpha bands and $NVC_{EEG \rightarrow HbO}$ in delta bands showed an increasing trend, while $NVC_{EEG \rightarrow HbO}$ in theta and alpha bands showed a decrease followed by an increase.

TABLE III

The $K_{EEG-fNIRS}$ of Causal Statistics for Different Brain Regions and Different Frequency Bands Under 0-Back, 2-Back, and 3-Back Conditions, and the p-Value Results of the Significance of ANOVA Analysis for Cognitive Load. (Different Brain Regions Are Denoted by EEG Channel Names)

Corresponding brain regions and frequency bands		EEG-HbR				EEG-HbO			
		0-back	2-back	3-back	p-value	0-back	2-back	3-back	p-value
AFz	Delta	0.196	0.192	0.191	0.548	0.248	0.188	0.225	**0.011**
	Theta	0.215	0.208	0.177	**0.008**	0.238	0.188	0.238	**0.046**
	Alpha	0.211	0.210	0.189	**0.002**	0.240	0.190	0.246	**<0.001**
	Beta	0.207	0.201	0.188	0.142	0.251	0.183	0.248	**<0.001**
	Gamma	0.208	0.192	0.183	0.066	0.248	0.187	0.243	**<0.001**
C3	Delta	0.217	0.237	0.195	0.089	0.198	0.201	0.215	0.102
	Theta	0.201	0.229	0.201	0.056	0.171	0.193	0.208	0.053
	Alpha	0.212	0.187	0.226	0.123	0.177	0.172	0.193	0.402
	Beta	0.193	0.220	0.215	**0.034**	0.176	0.170	0.196	0.129
	Gamma	0.203	0.208	0.169	0.195	0.1754	0.172	0.195	**0.001**
C4	Delta	0.220	0.233	0.203	0.123	0.164	0.195	0.210	0.079
	Theta	0.219	0.210	0.239	0.106	0.176	0.199	0.211	**0.001**
	Alpha	0.202	0.206	0.202	0.960	0.168	0.192	0.226	**<0.001**
	Beta	0.200	0.205	0.227	0.957	0.174	0.153	0.213	**<0.001**
	Gamma	0.216	0.221	0.214	0.775	0.174	0.163	0.199	**0.029**
POz	Delta	0.184	0.199	0.197	0.692	0.213	0.225	0.253	**0.01**
	Theta	0.180	0.185	0.218	**0.006**	0.213	0.185	0.263	**<0.001**
	Alpha	0.176	0.207	0.227	**0.004**	0.226	0.203	0.255	**<0.001**
	Beta	0.194	0.210	0.201	0.303	0.231	0.226	0.230	0.930
	Gamma	0.178	0.188	0.213	0.069	0.218	0.211	0.246	0.068

In the long-term analysis, $NVC_{EEG \to fNIRS}$ values were separately computed for 25 participants (participant 4 excluded due to data quality issues) using the CMVGP-CCM method. The Kruskal-Wallis test was used to assess statistical significance and compare the differences in causal strength across different tasks and frequency bands. In **Fig. 7**, $NVC_{EEG \to fNIRS}$ values showed that compared to the 0-back condition, the causal strength values of the 2-back condition are significantly reduced. As the difficulty of the n-back task increases, the low-frequency bands of EEG signals, including delta, theta, and alpha, exhibit stronger driving effects on fNIRS signals. In the 3-back condition, a few reverse causal drives (i.e., $NVC_{fNIRS \to EEG}$) were observed in alpha and gamma frequency bands. The Kruskal-Wallis non-parametric test showed that there is a significant difference in the $NVC_{EEG \to fNIRS}$ derived from the CMVGP-CCM between the 0-back, 2-back, and 3-back conditions. The post-hoc tests were conducted, and the corrected statistical results are shown in **Fig. 7**. $NVC_{EEG \to HbR}$ in the theta, beta, and gamma frequency bands under the 0-back condition showed significant differences to the 2-back and 3-back conditions. Compared to HbR, the differences in $NVC_{EEG \to HbO}$ under different experimental conditions were not obvious. In the 2-back condition, significant differences were observed in the delta and beta frequency bands (p=0.002).

IV. DISCUSSION

This study proposed the CMVGP-CCM-based analytical framework to investigate the neurovascular coupling between EEG and fNIRS signals under varying cognitive difficulty by capturing potential correlations between different components of EEG and fNIRS signals. The results of simulation experiments demonstrated that the CMVGP-CCM method can provide a more comprehensive description of the causal relationships between two modalities. In the real EEG-fNIRS casual analysis, we found that during WM, the EEG signal in the low-frequency bands had a significant causal influence on the fNIRS signal, with its strength decreasing as cognitive demands increased. Taken together, the proposed NVC analysis framework may stand as a superior method for the causal and neurovascular coupling analysis of EEG and fNIRS signals.

The proposed NVC analysis evaluated the causal relationship between EEG and fNIRS signals in different brain regions. We found that the causal drive from the middle prefrontal delta band to HbR decreases with the increase of cognitive load. This finding is expected since the delta band is believed to carry the information involved in WM, which is consistent with existing studies [45], [46]. In addition, the causal intensity changes in the left and right brain motor regions are lateralized. This finding is similar to existing studies [37], further confirming the feasibility of the proposed
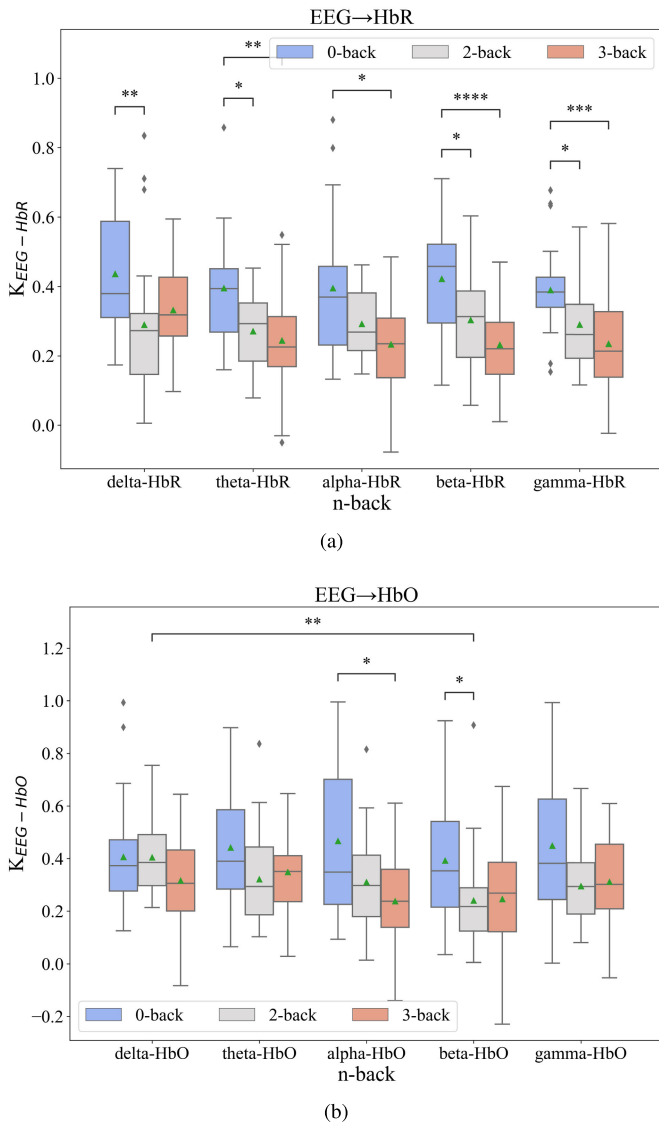
Fig. 7. The Causal driving strengths between EEG and fNIRS signals for different frequency bands and tasks in long-term sequence analysis. (a) From different frequency bands of EEG to HbR. (b) From different frequency bands of EEG to HbO. The green triangle represents the average value. The notation '****', '***', '**', '*' represents significance at the levels of $p<0.0001$, $p<0.001$, $p<0.01$, and $p<0.05$, respectively.

NVC method in the present study. In the case of increased cognitive load, causal drive in the parietal lobe showed a different trend compared to the middle prefrontal lobe, possibly due to enhanced memory and sensory representation in the parietal lobe by attention [47]. Overall, the proposed method has provided a promising capability for a deeper understanding of NVC under different cognitive conditions.

Secondly, we focused on the NVC in the middle prefrontal region. When participants engage in the *n*-back task, neurons in the WM-related brain regions become active and consume a large amount of energy, leading to an increase in HbO concentration and a decrease in HbR concentration, indicating the release of oxygen to meet the demands of neural activity. This theoretically suggests that changes in EEG drive fNIRS. Our experimental results also confirm this, which is consistent with existing research findings [35]. Extensive research

has shown [48], [49], [50] that delta rhythm is associated with the fatigue state of participants during the task, theta rhythm is related to long-term memory, and alpha rhythm plays an important role in attention regulation. In the 3-back condition, the driving effect of delta rhythm on HbR becomes more pronounced compared to other frequency bands. Low-frequency EEG signals play a major role in cognitive tasks, which is consistent with existing research findings [51]. Our results showed that the causal intensity from EEG to fNIRS spectrum decreased significantly with the increase of cognitive load. This may be related to the decreased activation degree of the midfrontal cortex region [52], [53], resulting in the weakened regulation of EEG to fNIRS spectrum. At the same time, we can speculate that the concentration of HbR and HbO might decrease with the increase in workload, and there may be a decline in the stability of brain control, thus leading to a weakening of the causal relationship between EEG and fNIRS.

To the best of our knowledge, it is worth mentioning, our experimental results provide the first causal analysis-based explanation for the significant differences in EEG-fNIRS coupling between the 0-back condition and the 2-back and 3-back conditions, while no significant differences were observed between the 2-back and 3-back conditions. This viewpoint has been partially reflected in previous WM classification studies based on EEG-fNIRS [54]. However, it does not explain the underlying reasons for this phenomenon. In addition, our results further support this observation by demonstrating the differential causal influence of EEG signals in the theta, beta, and gamma frequency bands on HbR concentration across different experimental conditions. Our method reveals the main direction of NVC under WM, explaining the differences in causal relationships between EEG and fNIRS across different frequency bands. This contributes to understanding the information exchange of physiological system under potential influencing variables, providing a new way to reveal the mechanism of NVC under cognitive load.

While this study has made some progress in the EEG-fNIRS coupling research of WM, there are still some limitations. In the study of multi-modal causal driving in the brain, there is no universal indicator to determine causal relationships, and CCM and its improved methods lack reliability under low coupling strength [55]. The proposed method improves the reliability of causal computation to some extent, particularly in scenarios with low coupling. However, simulation experiments revealed that compared to the CCM method, the CMVGP-CCM method generated lower estimates of coupling strength under short time series conditions. This may be because there are too few data points to accurately estimate the optimal parameter values. The CMVGP-CCM method extends the bivariate measure of relative causality to multivariate, which is a step forward. However, in the future, it is necessary to address the issue of memory consumption in multidimensional variables to achieve more accurate and faster causal strength calculations.

V. CONCLUSION

This paper proposed a CMVGP-CCM-based coupling analysis framework for the investigation of neurovascular coupling

between EEG and fNIRS in brain. Results of the simulation and real datasets demonstrated the effectiveness of our method. In particular, our study showed that EEG signals in the delta, theta, and alpha bands in WM revealed a stronger driving effect on fNIRS signals. This effect became stronger as the cognitive difficulty increased. These findings, though preliminary, seem to confirm that the direction of NVC in WM is from EEG to fNIRS signals. In the future, we expect that the proposed method can be further improved and applied to more applications.

REFERENCES

[1] D. Attwell, A. M. Buchan, S. Charpak, M. Lauritzen, B. A. MacVicar, and E. A. Newman, "Glial and neuronal control of brain blood flow," *Nature*, vol. 468, no. 7321, pp. 232–243, Nov. 2010.

[2] A. A. Phillips, F. H. Chan, M. M. Z. Zheng, A. V. Krassioukov, and P. N. Ainslie, "Neurovascular coupling in humans: Physiology, methodological advances and clinical implications," *J. Cerebral Blood Flow Metabolism*, vol. 36, no. 4, pp. 647–664, Apr. 2016, doi: 10.1177/0271678x15617954.

[3] S. Tarantini et al., "Treatment with the mitochondrial antioxidant peptide SS-31 rescues neurovascular coupling responses and cerebrovascular endothelial function and improves cognition in aged mice," *Aging Cell*, vol. 17, no. 2, Feb. 2018, Art. no. e12731.

[4] D. Perpetuini et al., "Working memory decline in Alzheimer's disease is detected by complexity analysis of multimodal EEG-fNIRS," *Entropy*, vol. 22, no. 12, p. 1380, Dec. 2020.

[5] T. Csipo et al., "Increased cognitive workload evokes greater neurovascular coupling responses in healthy young adults," *PLoS ONE*, vol. 16, no. 5, May 2021, Art. no. e0250043.

[6] A. M. Owen, K. M. Mcmillan, A. R. Laird, and E. Bullmore, "N-back working memory paradigm: A meta-analysis of normative functional neuroimaging studies," *Hum. Brain Mapping*, vol. 25, no. 1, pp. 46–59, 2005.

[7] P. Xie et al., "A multidimensional visible evaluation model for stroke rehabilitation: A pilot study," *IEEE Trans. Neural Syst. Rehabil. Eng.*, vol. 31, pp. 1721–1731, 2023.

[8] Q. She, G. Jin, R. Zhu, M. Houston, O. Xu, and Y. Zhang, "Upper limb cortical-muscular coupling analysis based on time-delayed back maximum information coefficient model," *IEEE Trans. Neural Syst. Rehabil. Eng.*, vol. 31, pp. 4635–4643, 2023.

[9] Y. Gao, H. Su, R. Li, and Y. Zhang, "Synchronous analysis of brain regions based on multi-scale permutation transfer entropy," *Comput. Biol. Med.*, vol. 109, pp. 272–279, Jun. 2019.

[10] Q. She, Y. Cai, S. Du, and Y. Chen, "Multi-source manifold feature transfer learning with domain selection for brain–computer interfaces," *Neurocomputing*, vol. 514, pp. 313–327, Dec. 2022.

[11] R. Li, G. Rui, W. Chen, S. Li, P. E. Schulz, and Y. Zhang, "Early detection of Alzheimer's disease using non-invasive near-infrared spectroscopy," *Frontiers Aging Neurosci.*, vol. 10, p. 366, Nov. 2018.

[12] R. Li, G. Rui, C. Zhao, C. Wang, F. Fang, and Y. Zhang, "Functional network alterations in patients with amnestic mild cognitive impairment characterized using functional near-infrared spectroscopy," *IEEE Trans. Neural Syst. Rehabil. Eng.*, vol. 28, no. 1, pp. 123–132, Jan. 2020.

[13] Y. Gao, B. Jia, M. Houston, and Y. Zhang, "Hybrid EEG-fNIRS brain computer interface based on common spatial pattern by using EEG-informed general linear model," *IEEE Trans. Instrum. Meas.*, vol. 72, 2023, Art. no. 4006110.

[14] R. Li, C. Zhao, C. Wang, J. Wang, and Y. Zhang, "Enhancing fNIRS analysis using EEG rhythmic signatures: An EEG-informed fNIRS analysis study," *IEEE Trans. Biomed. Eng.*, vol. 67, no. 10, pp. 2789–2797, Oct. 2020.

[15] R. Li, T. Potter, W. Huang, and Y. Zhang, "Enhancing performance of a hybrid EEG-fNIRS system using channel selection and early temporal features," *Frontiers Human Neurosci.*, vol. 11, p. 462, Sep. 2017.

[16] R. Li, T. Nguyen, T. Potter, and Y. Zhang, "Dynamic cortical connectivity alterations associated with Alzheimer's disease: An EEG and fNIRS integration study," *NeuroImage Clin.*, vol. 21, Jan. 2019, Art. no. 101622.

[17] R. Li, D. Yang, F. Fang, K.-S. Hong, A. L. Reiss, and Y. Zhang, "Concurrent fNIRS and EEG for brain function investigation: A systematic, methodology-focused review," *Sensors*, vol. 22, no. 15, p. 5865, Aug. 2022.

[18] P. A. Cicalese et al., "An EEG-fNIRS hybridization technique in the four-class classification of Alzheimer's disease," *J. Neurosci. Methods*, vol. 336, Apr. 2020, Art. no. 108618.

[19] Y. Gao, H. Liu, F. Fang, and Y. Zhang, "Classification of working memory loads via assessing broken detailed balance of EEG-FNIRS neurovascular coupling measures," *IEEE Trans. Biomed. Eng.*, vol. 70, no. 3, pp. 877–887, Mar. 2023.

[20] K. Suzuki, Y. Okumura, Y. Kita, Y. Oi, H. Shinoda, and M. Inagaki, "The relationship between the superior frontal cortex and alpha oscillation in a flanker task: Simultaneous recording of electroencephalogram (EEG) and near infrared spectroscopy (NIRS)," *Neurosci. Res.*, vol. 131, pp. 30–35, Jun. 2018.

[21] Y. Kaga et al., "Executive dysfunction in medication-Naïve children with ADHD: A multi-modal fNIRS and EEG study," *Brain Develop.*, vol. 42, no. 8, pp. 555–563, Sep. 2020.

[22] H. Dashtestani et al., "Structured sparse multiset canonical correlation analysis of simultaneous fNIRS and EEG provides new insights into the human action-observation network," *Sci. Rep.*, vol. 12, no. 1, p. 6878, Apr. 2022.

[23] A. M. Chiarelli et al., "Evidence of neurovascular un-coupling in mild Alzheimer's disease through multimodal EEG-fNIRS and multivariate analysis of resting-state data," *Biomedicines*, vol. 9, no. 4, p. 337, Mar. 2021.

[24] I. Cohen, Y. Huang, J. Chen, and J. Benesty, "Pearson correlation coefficient," in *Noise Reduction in Speech Processing*. Berlin, Germany: Springer, 2009, pp. 1–4.

[25] A. Kraskov, H. Stögbauer, and P. Grassberger, "Estimating mutual information," *Phys. Rev. E, Stat. Phys. Plasmas Fluids Relat. Interdiscip. Top.*, vol. 69, no. 6, Jun. 2004, Art. no. 066138.

[26] S. B. Borghei et al., "Multimodal exploration of non-motor neural functions in ALS patients using simultaneous EEG-fNIRS recording," *J. Neural Eng.*, vol. 16, no. 6, Nov. 2019, Art. no. 066036.

[27] G. Sugihara et al., "Detecting causality in complex ecosystems," *Science*, vol. 338, no. 6106, pp. 496–500, Oct. 2012.

[28] K. Schiecke et al., "Nonlinear directed interactions between HRV and EEG activity in children with TLE," *IEEE Trans. Biomed. Eng.*, vol. 63, no. 12, pp. 2497–2504, Dec. 2016, doi: 10.1109/TBME.2016.2579021.

[29] H. Natsukawa and K. Koyamada, "Visual analytics of brain effective connectivity using convergent cross mapping," in *Proc. SIGGRAPH Asia Symp. Visualizat.*, Nov. 2017, pp. 1–9.

[30] A. Chowdhury, D. Dewan, L. Ghosh, A. Konar, and A. K. Nagar, "Brain connectivity analysis in color perception problem using convergent cross mapping technique," in *Soft Computing for Problem Solving*, vol. 1. Singapore: Springer, 2020, pp. 287–299.

[31] S. Avvaru and K. K. Parhi, "Effective brain connectivity extraction by frequency-domain convergent cross-mapping (FDCCM) and its application in Parkinson's disease classification," *IEEE Trans. Biomed. Eng.*, vol. 70, no. 8, pp. 2475–2485, Feb. 2023, doi: 10.1109/TBME.2023.3250355.

[32] A. Ghouse, L. Faes, and G. Valenza, "Inferring directionality of coupled dynamical systems using Gaussian process priors: Application on neurovascular systems," *Phys. Rev. E, Stat. Phys. Plasmas Fluids Relat. Interdiscip. Top.*, vol. 104, no. 6, Dec. 2021, Art. no. 064208.

[33] A. D. Bahamonde, R. M. Montes, and P. Cornejo, "Usefulness and limitations of convergent cross sorting and continuity scaling methods for their application in simulated and real-world time series," *Royal Soc. Open Sci.*, vol. 10, no. 7, Jul. 2023, Art. no. 221590.

[34] S. K. Stavroglou, A. A. Pantelous, H. E. Stanley, and K. M. Zuev, "Hidden interactions in financial markets," *Proc. Nat. Acad. Sci. USA*, vol. 116, no. 22, pp. 10646–10651, 2019.

[35] X. Ge and A. Lin, "Symbolic convergent cross mapping based on permutation mutual information," *Chaos, Solitons Fractals*, vol. 167, Feb. 2023, Art. no. 112992.

[36] A. Ghouse and G. Valenza, "Inferring parsimonious coupling statistics in nonlinear dynamics with variational Gaussian processes," in *Proc. Int. Conf. Complex Netw. Their Appl.* Cham, Switzerland: Springer, 2022, pp. 377–389.

[37] J. Shin et al., "Simultaneous acquisition of EEG and NIRS during cognitive tasks for an open access dataset," *Sci. Data*, vol. 5, no. 1, pp. 1–16, Feb. 2018.

[38] L. Michels, M. Moazami-Goudarzi, D. Jeanmonod, and J. Sarnthein, "EEG alpha distinguishes between cuneal and precuneal activation in working memory," *NeuroImage*, vol. 40, no. 3, pp. 1296–1310, Apr. 2008.

[39] A. Delorme and S. Makeig, "EEGLAB: An open source toolbox for analysis of single-trial EEG dynamics including independent component analysis," *J. Neurosci. Methods*, vol. 134, no. 1, pp. 9–21, Mar. 2004.

[40] B. Blankertz et al., "The Berlin brain–computer interface: Progress beyond communication and control," *Frontiers Neurosci.*, vol. 10, Nov. 2016, Art. no. 205839.

[41] M. S. Hossain et al., "Motion artifacts correction from EEG and fNIRS signals using novel multiresolution analysis," *IEEE Access*, vol. 10, pp. 29760–29777, 2022.

[42] G. Sugihara and R. M. May, "Nonlinear forecasting as a way of distinguishing chaos from measurement error in time series," *Nature*, vol. 344, no. 6268, pp. 734–741, Apr. 1990.

[43] D. J. C. MacKay, "Bayesian methods for backpropagation networks," in *Models of Neural Networks III: Association, Generalization, and Representation*. New York, NY, USA: Springer, 1996, pp. 211–254.

[44] D. Mønster, R. Fusaroli, K. Tylén, A. Roepstorff, and J. F. Sherson, "Causal inference from noisy time-series data—Testing the convergent cross-mapping algorithm in the presence of noise and external influence," *Future Gener. Comput. Syst.*, vol. 73, pp. 52–62, Aug. 2017.

[45] P. Zarjam, J. Epps, and F. Chen, "Characterizing working memory load using EEG delta activity," in *Proc. 19th Eur. Signal Process. Conf.*, Aug. 2011, pp. 1554–1558.

[46] S. Wang, J. Gwizdka, and W. A. Chaovalitwongse, "Using wireless EEG signals to assess memory workload in the *n*-back task," *IEEE Trans. Human-Mach. Syst.*, vol. 46, no. 3, pp. 424–435, Jun. 2016.

[47] M. F. Panichello and T. J. Buschman, "Shared mechanisms underlie the control of working memory and attention," *Nature*, vol. 592, no. 7855, pp. 601–605, Apr. 2021.

[48] S. Zhu, Z. Fang, S. Hu, Z. Wang, and H. Rao, "Resting state brain function analysis using concurrent BOLD in ASL perfusion fMRI," *PLoS ONE*, vol. 8, no. 6, Jun. 2013, Art. no. e65884.

[49] J. I. F. Bass, A. Diallo, J. Nelson, J. M. Soto, C. L. Myers, and A. J. M. Walhout, "Using networks to measure similarity between genes: Association index selection," *Nature Methods*, vol. 10, no. 12, pp. 1169–1176, Dec. 2013.

[50] M. Levandowsky and D. Winter, "Distance between sets," *Nature*, vol. 234, no. 5323, pp. 34–35, Nov. 1971.

[51] J. Lin, J. Lu, Z. Shu, N. Yu, and J. Han, "An EEG-fNIRS neurovascular coupling analysis method to investigate cognitive-motor interference," *Comput. Biol. Med.*, vol. 160, Jun. 2023, Art. no. 106968.

[52] Y. Liu, H. Ayaz, and P. A. Shewokis, "Multisubject 'learning' for mental workload classification using concurrent EEG, fNIRS, and physiological measures," *Frontiers Hum. Neurosci.*, vol. 11, p. 389, Jul. 2017.

[53] A. Miró-Padilla, E. Bueichekú, N. Ventura-Campos, M.-J. Flores-Compañ, M. A. Parcet, and C. Ávila, "Long-term brain effects of N-back training: An fMRI study," *Brain Imag. Behav.*, vol. 13, no. 4, pp. 1115–1127, Aug. 2019.

[54] J. Cao, E. M. Garro, and Y. Zhao, "EEG/fNIRS based workload classification using functional brain connectivity and machine learning," *Sensors*, vol. 22, no. 19, p. 7623, Oct. 2022.

[55] S. Bartsev, M. Saltykov, P. Belolipetsky, and A. Pianykh, "Imperfection of the convergent cross-mapping method," *Proc. IOP Conf. Ser., Mater. Sci. Eng.*, vol. 1047, no. 1, 2021, Art. no. 012081.